REVISTA DCS
FUNDADA EN 2000

CONTROL AND CURRENT HARMONIC FILTERING FOR GRID CONNECTED WIND TURBINE ENERGY SYSTEMS WITH DOUBLE-FED INDUCTION GENERATOR

CONTROLE E FILTRAGEM DE HARMÔNICOS DE CORRENTE PARA SISTEMAS DE ENERGIA EÓLICA CONECTADOS À REDE COM GERADOR DE INDUÇÃO DE DUPLA ALIMENTAÇÃO

CONTROL Y FILTRADO DE ARMÓNICOS DE CORRIENTE PARA SISTEMAS DE ENERGÍA EÓLICA CONECTADOS A LA RED CON GENERADOR DE INDUCCIÓN DE DOBLE ALIMENTACIÓN

Marco Aurélio Rocha[1], Guilherme Augusto Marabezzi Clerice[2], Douglas Ricardo Fumes[3], Bruno Henrique da Silveira[4]

DOI: 10.54899/dcs.v23i87.4536
Recibido: 09/01/2026 | Aceptado: 30/01/2026 | Publicación en línea: 09/02/2026.

ABSTRACT

This paper presents the modelling and simulating of a general wind power system with double-fed induction generator controlled by a back-to-back converter, in order to manage power delivery to or absorbed from the grid through reactive compensation and active filtering of electrical current. The system modelling and the controller design was developed in Matlab®/Simulink® software, where the rotor-side converter control regulates torque and controls active and reactive power. The grid-side converter control maintains the DC link voltage constant and compensates reactive power demanded from the load, besides this converter acts as an active power filter, which improves the total harmonic distortion of the grid current. The main difference of the proposed methodology with respect to others in the literature is the implementation of grid side converter control as an active power filter using proportional integral resonant to mitigate the 5ª, 7ª, 11ª and 13ª harmonics instead of simple Proportional-Integral (PI) controller, which reduces the accomplishment difficulties since the decoupled term is eliminated. The results obtained shows the correction of the power factor and the extraction of the maximum power from the wind. Finally, it is shown harmonic compensation for nonlinear loads and improvement of the total harmonic distortion of the grid current.

Keywords: Wind Power System. Reactive Power Compensation. Active Power Filtering. Back-to-back Converter. Double Fed Induction Generator (DFIG). Power Quality.

[1] PhD in Electrical Engineering, Universidade Estadual Paulista "Júlio de Mesquita Filho" (UNESP), Botucatu, São Paulo, Brazil. E-mail: marco.rocha@unesp.br
[2] PhD in Electrical Engineering, Universidade Estadual Paulista "Júlio de Mesquita Filho" (UNESP), Botucatu, São Paulo, Brazil. E-mail: guilherme.augusto@sp.senai.br
[3] Master in Mechanical Engineering, Universidade Estadual Paulista "Júlio de Mesquita Filho" (UNESP), Botucatu, São Paulo, Brazil. E-mail: douglas.fumes@gmail.com
[4] Master in Mechanical Engineering, Universidade Estadual Paulista "Júlio de Mesquita Filho" (UNESP), Avaré, São Paulo, Brazil. E-mail: brunoh.silveira@hotmail.com

RESUMO

Este artigo apresenta a modelagem e simulação de um sistema geral de energia eólica com gerador de indução de dupla alimentação controlado por um conversor back-to-back, com o objetivo de gerenciar a potência fornecida à rede ou absorvida dela por meio de compensação reativa e filtragem ativa da corrente elétrica. A modelagem do sistema e o projeto do controlador foram desenvolvidos no software Matlab®/Simulink®, onde o controle do conversor do lado do rotor regula o torque e controla a potência ativa e reativa. O controle do conversor do lado da rede mantém a tensão do barramento CC constante e compensa a potência reativa demandada da carga; além disso, este conversor atua como um filtro ativo de potência, o que melhora a distorção harmônica total da corrente da rede. A principal diferença da metodologia proposta em relação a outras na literatura é a implementação do controle do conversor do lado da rede como um filtro ativo de potência usando um controlador proporcional-integral ressonante para mitigar as harmônicas de 5ª, 7ª, 11ª e 13ª ordem, em vez de um controlador proporcional-integral (PI) simples, o que reduz as dificuldades de implementação, uma vez que o termo desacoplado é eliminado. Os resultados obtidos demonstram a correção do fator de potência e a extração da potência máxima do vento. Por fim, é apresentada a compensação harmônica para cargas não lineares e a melhoria da distorção harmônica total da corrente da rede.

Palavras-chave: Sistema de Energia Eólica. Compensação de Potência Reativa. Filtragem de Potência Ativa. Conversor Back-to-back. Gerador de Indução de Dupla Alimentação (DFIG). Qualidade de Energia.

RESUMEN

Este artículo presenta el modelado y la simulación de un sistema eólico general con un generador de inducción de doble alimentación controlado por un convertidor back-to-back, con el fin de gestionar la potencia suministrada o absorbida de la red mediante la compensación reactiva y el filtrado activo de la corriente eléctrica. El modelado del sistema y el diseño del controlador se desarrollaron en el software Matlab®/Simulink®, donde el control del convertidor del lado del rotor regula el par y controla la potencia activa y reactiva. El control del convertidor del lado de la red mantiene constante la tensión del enlace de CC y compensa la potencia reactiva demandada por la carga. Además, este convertidor actúa como un filtro de potencia activa, lo que mejora la distorsión armónica total de la corriente de la red. La principal diferencia de la metodología propuesta con respecto a otras publicadas en la literatura radica en la implementación del control del convertidor del lado de la red como un filtro de potencia activa que utiliza un resonante proporcional-integral para mitigar los armónicos 5ª, 7ª, 11ª y 13ª, en lugar de un simple controlador proporcional-integral (PI), lo que reduce las dificultades de implementación al eliminar el término desacoplado. Los resultados obtenidos muestran la corrección del factor de potencia y la extracción de la máxima potencia eólica. Finalmente, se muestra la compensación armónica para cargas no lineales y la mejora de la distorsión armónica total de la corriente de red.

Palabras clave: Sistema Eólico. Compensación de Potencia Reactiva. Filtrado de Potencia Activa. Convertidor Back-to-back. Generador de Inducción de Doble Alimentación (DFIG). Calidad de la Energía.

INTRODUCTION

In a scenario of great worldwide development, the electricity demand has been gradually increasing so that conventional energy sources, such as the ones derived from fossil fuels, undergo constantly price oscillations, offering financial and technical-economic risks. Furthermore, concern with the environment related to the emission of polluting gases into the atmosphere and global warming has been intensified. In this sense, many countries have exploited the usage of alternative energy sources, among which the wind stands out due to its economic viability with competitive costs in $/kWh. On the other hand, the main issue with renewable energy sources is their stochastic feature, in other words, the power is not always available when it is needed (BUBSHAIT, A.S. et al., 2017; ACKERMANN, T., 2012). With the increase of power production from variable speed wind systems, especially for those dominated by double fed induction generator (DFIG), and the large implementation of utility integration, power electronic devices as converters have been used to control active and reactive power flow, frequency and to support the electrical system during disturbances, including faults and voltage sags (MOREIRA, A.B. *et al.*, 2017; TIAN, X., *et. al*, 2017; MEEGAHAPOLA L. and FLYNN, D., 2010).

Besides, power quality has become an essential aspect not only for wind power installation, but also for any system that presents power electronic converters connected to the grid, which results in injection of harmonic current on the electrical system. This grid pollution causes voltage and current waveform distortions, in addition low power factor, possible warming, flicker effect, among others (MOREIRA, A. B. *et, al*, 2017; RASHID, M. H., 2013). Double fed induction generator based wind turbines can be connected to the grid through a back-to-back converter topology, which allows the design of controllers in both of rotor side and grid side converters (RSC and GSC, respectively). Several control approaches have been introduced in the literature with RSC designed to extract the maximum power point from wind and GSC to ensure the delivery of active and reactive power to the grid (BUBSHAIT, A. S. *et al*, 2017; TAPIA, A. *et al*, 2003). Moreover, the grid side converter admits also the active power filtering (APF), which detects the harmonic electric current of nonlinear loads at the point of common coupling (PCC) and compensates it to improve the power quality supplied. Inversely, mitigation of grid harmonic current by means of the rotor side converter injects harmonics on DFIG, which may occasion problems, such as increase of losses and reduction of the machine service life (MOREIRA, A. B. *et al*, 2017; BOUTOUBAT, M. *et al*, 2012).

Aiming to develop feasible wind energy systems connected to the grid, the mainstream control strategies for DFIG in literature are vector control (VC) and direct power control (DPC). DPC methods have as features low machine parameters dependence and high dynamic performance besides of simple structure. On the other hand, DPC produces large power ripples and the control accuracy is not satisfactory because of the voltage vector selection from a fixed switching table (WANG, X. *et al*, 2017; SINGH B. and NAIDU, N. K. S., 2014). The VC strategy presents great steady-state performance due to its space vector modulation technique, apart from decomposing the currents into active and reactive components, which allows decoupled control loops. However, it may not guarantee a suitable dynamic performance once the PIs produce lag effect as well as they need much parameter tuning work. In addition, a phase-locked loop (PLL) is also needed to change the system into synchronous reference frame WANG, *et al*, 2017.; SUN, D. and WANG, X., 2016; SUN, D. *et al*, 2018; AKAGI H. and SATO, H., 2002). The most widespread technique is based on flow-oriented vector control, which requires a precise synchronization to the stator flow vector to control active and reactive power through direct and quadrature (d-q) axis components of rotor currents.

In order to accomplish the harmonic compensation of electric current, the studies on DFIG converters operating additionally as APF show that it can be done by three different methods: using GSC for harmonic compensation as standard shunt active filter; using RSC for canceling the harmonics; and using a combination of both GSC and RSC to divide the harmonic power flow between the converters. Although it is possible to compensate harmonics based on RSC (LÓPEZ-NÚÑEZ *et al.*, 2016), subjecting the DFIG system as an active power filter results in higher power losses and not adequate machine operation (TODESCHINI; EMANUEL, 2010). Lately, some studies have implemented the current harmonic based on GSC and the Synchronous Reference Frame (SRF) control method to extract the fundamental component of load currents (MOREIRA *et al.*, 2017; NAIDU; SINGH, 2015). In Moreira *et al.* (2017), the authors propose a strategy for power control besides the power quality improvement by using the GSC to perform active filtering at the PCC with the presence of a three-phase full bridge rectifier feeding a resistive load. The APF function is performed using d-q reference frame and proportional integral compensator.

In this context, this paper proposes a control structure based on Proportional Integral

Resonant (PIR) controller for the GSC, which reduces the harmonic content originated by converter commutation and the voltage ripple of DC link, performs the active power filtering function, as well as controls the active and reactive power flow. In order to analyze the results of the proposed method, it was chosen Currents' Physical Components (CPC) theory due to his research relevance in scientific community. Computational results are presented to demonstrate the efficiency of this proposal. The organization is as follows: Section II briefly addresses the case of study. In section III, a succinct review of the CPC theory for three-phase circuits is presented. Section IV presents the mathematical model of DFIGURE Section V is dedicated to the control design of the back-to-back converter system and of the active power filter. In Section VI, simulation results are presented and, finally, section VII presents the conclusion of this paper.

System Configuration

Figure 1 shows the diagram of the system addressed in this paper. The wind turbine system is connected to the grid through a back-to-back converter with a double fed induction generator. At the point of common coupling, there are loads which are a combination of linear and non-linear loads causing harmonics and reactive power consumption.

Figure 1. Operation diagram of proposed wind system with DFIG/APF.

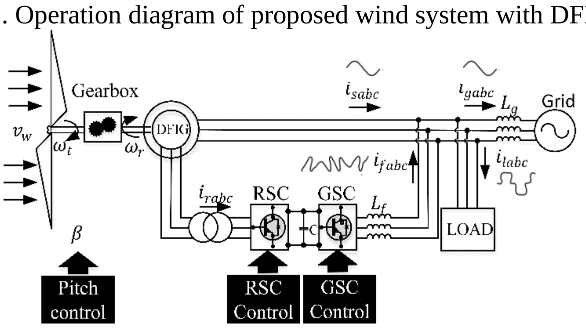

Source: Author

Currents' Physical Components Theory

The CPC theory, proposed by Czarnecki, is developed in frequency domain and is being constantly improved by the author in order to be applied under different conditions, such as symmetric and asymmetric, sinusoidal and distorted, balanced and unbalanced circuits, feeding linear and non-linear loads. This theory proposes separating the electric current into different components, each one related to distinct physical phenomena.

Assuming a generic three-wire three-phase system with harmonic generating load (HGL), due to its non-linearity of periodic time variance, it can become the source of energy at some harmonic frequencies, which means that active power flow is from load to source. Considering such behavior, the set of N harmonics can be divided into two groups, NG being the harmonics generated by the load and NC being the ones consumed by the load. As result, the current can be decomposed into the components called generated iG and consumed iC, as follows:

$$i = \sum_{n \in N} i_n = \sum_{n \in N_G} i_n + \sum_{n \in N_C} i_n = i_G + i_C \qquad (1)$$

When the system presents unbalanced loads, there are effects on the behavior of i_C, which can be calculated from the equivalent admittance Y_{bn}:

$$Y_{bn} = \frac{S_n^*}{\|u_n\|^2} = \frac{P_n - j.Q_n}{\|u_n\|^2} = G_{bn} + j.B_{bn} \qquad (2)$$

Consequently, the consumed current i_C can be decomposed into balanced and unbalanced components, obtained from:

$$i_b = \sqrt{2}\mathrm{Re} \sum_{n \in N_C} Y_{bn}.U_n.e^{j.n.w_1.t} \qquad (3)$$

$$i_u = i_C - i_b \qquad (4)$$

Each harmonic order of the balanced current i_b is composed of two parts, one in phase with the corresponding voltage harmonic, which is responsible by the active part of the power of the same harmonic and represented by the conductance G_{bn}; and another lagged of 90º of the corresponding voltage harmonic, responsible for the reactive portion of the power of the same harmonic and represented by the susceptance B_{bn}. The harmonic sum of the reactive portions is indeed the reactive current i_r, although the harmonic sum of the active portions i_{an} is not the active current:

$$i_r = \sqrt{2}\mathrm{Re} \sum_{n \in N_C} j.B_{bn}.U_n.e^{j.n.w_1.t} \qquad (5)$$

$$i_{an} = \sqrt{2}\mathrm{Re} \sum_{n \in N_C} G_{bn}.U_n.e^{j.n.w_1.t} \qquad (6)$$

Furthermore, the active current can also be separated into two components, one called active current i_a, related to the equivalent conductance G_e, and another one called scattered current i_s, discovered by Czarnecki, named so due to the dispersion of conductance values G_{bn} around of equivalent G_e:

$$i_a = G_e.u_C = \frac{P_C}{\|u_C\|^2}.u_C = \frac{\sum_{n \in N_C} P_n}{\sum_{n \in N_C}\|u_n\|^2}.u_C \qquad (7)$$

$$i_s = i_{an} - i_a = \sqrt{2}\mathrm{Re} \sum_{n \in N_C} (G_{bn} - G_e).U_n.e^{j.n.w_1.t} \qquad (8)$$

Once the resulting components are mutually orthogonal, their rms values obey the following relation:

$$\|i\|^2 = \|i_a\|^2 + \|i_s\|^2 + \|i_r\|^2 + \|i_u\|^2 + \|i_G\|^2 \qquad (9)$$

Multiplying (8) by the square of voltage rms value $\|u\|^2$, the power equation is obtained:

$$S^2 = P_a^2 + D_s^2 + Q_r^2 + D_u^2 + D_G^2 \qquad (10)$$

Double Fed Induction Generator and Wind Turbine Modelling

The electrical dynamics of DFIG are presented in (11)-(21) and its parameters are summarized in the appendix. The three-phase voltage equations from rotor and stator are obtained from (BOSE, 2001):

$$v_{abcs} = R_s i_{abcs} + \frac{d\lambda_{abcs}}{dt} \quad (11)$$

$$v_{abcr} = R_r i_{abcr} + \frac{d\lambda_{abcr}}{dt} \quad (12)$$

Eq. (11) and (12) can be described in the d-q reference frame, as follows:

$$v_{qs} = R_s i_{qs} + \omega\lambda_{ds} + \frac{d\lambda_{qs}}{dt} \quad (13)$$

$$v_{ds} = R_s i_{ds} - \omega\lambda_{qs} + \frac{d\lambda_{ds}}{dt} \quad (14)$$

$$v_{qr}' = R_r' i_{qr}' + (\omega_s - \omega_r)\lambda_{dr}' + \frac{d\lambda_{qr}'}{dt} \quad (15)$$

$$v_{dr}' = R_r' i_{dr}' - (\omega_s - \omega_r)\lambda_{qr}' + \frac{d\lambda_{dr}'}{dt} \quad (16)$$

Where the slip is the difference between the synchronous speed and the rotor one:

$$(\omega_s - \omega_r) = \omega_{slip} \quad (17)$$

The equations of rotor and stator magnetic fluxes are given as a function of the inductances and currents of the machine, as follows:

$$\lambda_{qs} = L_s i_{qs} + L_m i_{qr} \quad (18)$$

$$\lambda_{ds} = L_s i_{ds} + L_m i_{dr} \quad (19)$$

$$\lambda_{qr} = L_r i_{qr} + L_m i_{qs} \quad (20)$$

$$\lambda_{dr} = L_r i_{dr} + L_m i_{ds} \quad (21)$$

Where L_s, L_r and L_m are stator, rotor and magnetizing per phase inductances. The electromechanical dynamics of DFIG are shown in (22) and (23), where the electromagnetic torque is obtained from (BOSE, 2001):

$$T_e=\left(\frac{3}{2}\right)p\left(\lambda_{ds}i_{qs}-\lambda_{qs}i_{ds}\right) \qquad (22)$$

Where p is the number of poles. The dynamic of the mechanic system is expressed by:

$$J\frac{d\omega_m}{dt}=T_m-T_e-B\omega_m \qquad (23)$$

Where J is the moment of inertia, B is the coefficient of viscous friction of the system and T_m is the load torque. Finally, the active and reactive power can be described in (24)-(27) as (PENA; CLARE; ASHER, 1996):

$$P_s=\frac{3}{2}(v_{ds}i_{ds}+v_{qs}i_{qs}) \qquad (24)$$

$$P_r=\frac{3}{2}(v_{dr}'i_{dr}'+v_{qr}'i_{qr}') \qquad (25)$$

$$Q_s=\frac{3}{2}(v_{qs}i_{ds}-v_{ds}i_{qs}) \qquad (26)$$

$$Q_r=\frac{3}{2}(v_{qr}'i_{dr}'-v_{dr}'i_{qr}') \qquad (27)$$

Control Design

Rotor Side Controller

The main objective of rotor side converter is to make the torque and speed regulation of double fed induction generator, ensuring that the machine operates in sub-synchronous as well as super-synchronous speed.

The control system can be divided into two levels: external control loop, which is responsible for controlling the reactive power in the machine stator and the rotor angular speed, which generates the quadrature current reference to the internal control loop, i.e. to the current controller.

From (29) to (37), it is possible to obtain the control diagram shows the proposed scheme to RSC.

The proposed strategy is based on stator flux oriented vector control, which provides total decoupling of direct and quadrature axis. Figure 3 shows the vector diagram with induction machine variables (BOSE, 2001).

Figure 2. Control scheme of rotor side converter.

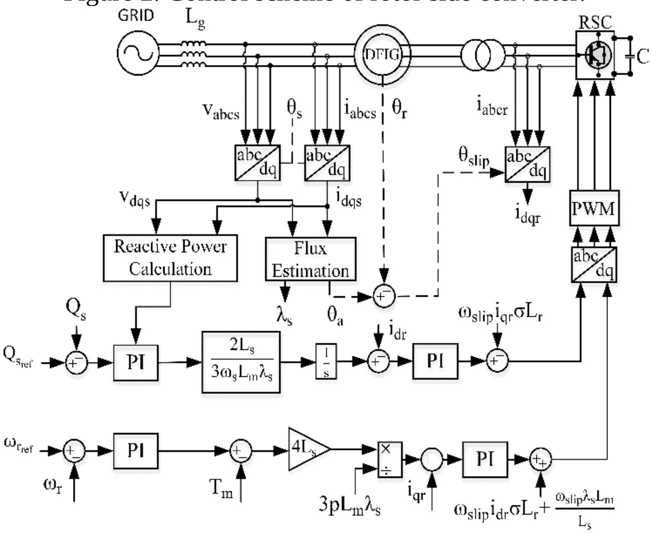

Source: Author

Where:

$$\sigma = 1 - \frac{L_m^2}{L_s L_r} \quad (28)$$

Figure 3. Vector diagram for stator flux orientation.

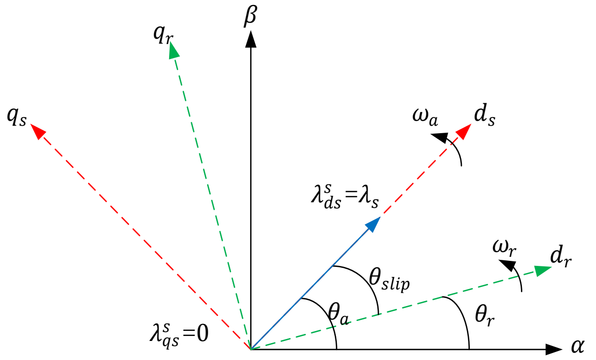

Source: Author

Where θ_a is the instantaneous angle of stator flux and ω_a is its angular speed. In steady state, stator flux is proportional to grid voltage and, since direct and quadrature stator fluxes keep constant, one can regard (PENA; CLARE; ASHER, 1996; CLARKE, 1943):

$$R_s = 0 \quad (29)$$

$$\frac{d\lambda_{ds}^s}{dt} = \frac{d\lambda_{qs}^s}{dt} = 0 \quad (30)$$

Consequently, it is possible to obtain d-q stator voltages from (13) and (14):

$$v_{ds} = 0 \quad (31)$$

$$v_{ds} = \omega\lambda_{ds} \quad (32)$$

Eq. (18) and (21) can be rewritten in order to express the relation between stator and rotor currents:

$$i_{ds} = \frac{\lambda_s - L_m i_{dr}'}{L_s} \quad (33)$$

$$i_{qs} = -\frac{L_m i_{qr}'}{L_s} \quad (34)$$

Replacing (33) and (34) in (24) and (26), one can obtain the active and reactive power available on stator machine controlled by the quadrature components of rotor current:

$$P_s = -\frac{3}{2}\frac{L_m}{L_s} v_{qs} i_{qr} \qquad (35)$$

$$Q_s = \frac{3}{2}\frac{L_m}{L_s} v_{qs}\left(\frac{v_{qs}}{\omega_a L_m} - i_{dr}\right) \qquad (36)$$

The phase locked loop is responsible for the synchronization between the grid voltage and the one produced by the converter, which generates an angle in phase with the grid voltage. The detail of the design procedure is presented in (NAM *et al.*, 2017). Figure 4 shows the PLL control scheme, which provides θ_a, where FLC is a fuzzy logic controller and MAF is a media average filter:

Figure 4. Achievement of flux position through PLL control.

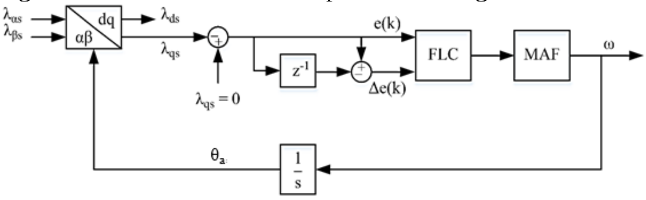

Source: Author

As the vector control is oriented by the stator flux, the electromagnetic torque in (22) can be obtained from (34) as:

$$T_e = -\left(\frac{3}{2}\right) p \left(\frac{L_m}{L_s}\right) \lambda_{ds} i_{qr}' \qquad (37)$$

Grid Side Controller

The main objective of grid side converter is to ensure the delivery of active and reactive power to the grid. Besides, the control structure of GSC keeps dc link voltage constant, regardless of power flux direction in rotor circuit.

The control system can be also divided into two levels: external control loop, which is responsible for controlling the dc link voltage and the delivery of reactive power, besides generating the stationary current reference (α-β) to the Proportional Integral Resonant controller of the internal loop through Clarke transformation. The current controller in internal loop provides more simplicity to the control design and decrease of dc voltage ripple. Figure 5 shows the scheme proposed to GSC.

Figure 5. Control scheme of grid side converter.

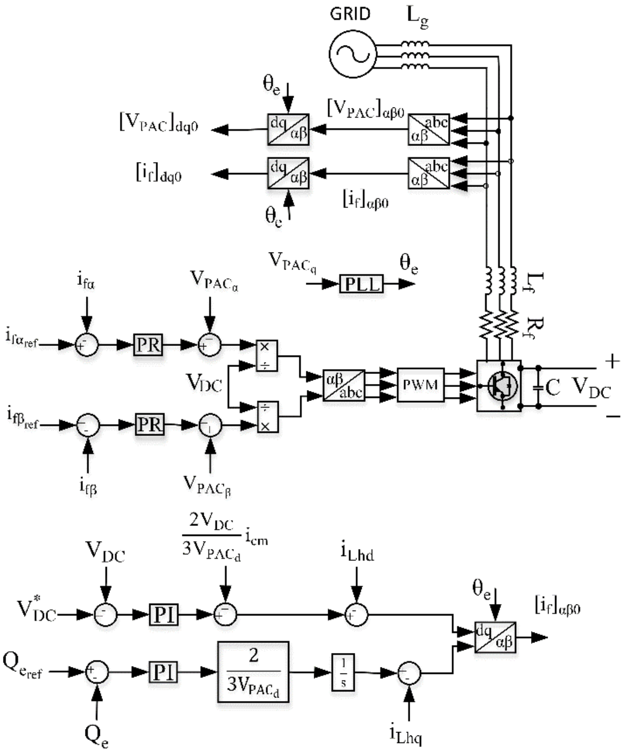

Source: Author

In the inner loop, there is a modification of the standard control model to mitigate harmonic currents coming from non-linear loads in the PCC of electric grid, as it will be shown in the next section. The control design methodology is described in (38) to (53).

The three-phase voltage equations from GSC are obtained from:

$$v_{abcg} = R_f i_{abcf} + L_f \frac{di_{abcf}}{dt} + d_{abc} V_{DC} \tag{38}$$

Where L_f is the filter inductance, R_f is the ohmic loss of the inductor and d is the duty cycle of the inverter neglecting the switch losses. It is shown that the grid side converter unit is controlled in α-β reference frame, then (38) can be rewritten:

$$v_{\alpha\beta g} = R_f i_{\alpha\beta f} + L_f \frac{di_{\alpha\beta f}}{dt} + d_{\alpha\beta} V_{DC} \qquad (39)$$

Considering grid voltage as the system disturbance, the transfer function that relates current and duty cycle is obtained from (39) in continuous plane “s”:

$$\frac{i_{\alpha f}}{d_\alpha} = \frac{i_{\beta f}}{i_\beta} = G_{i\alpha\beta f}(s) = -\frac{V_{DC}}{R + sL} \qquad (40)$$

The PIR controller is tuned to 5ª, 7ª, 11ª e 13ª harmonic orders and it also attenuates harmonics that may be caused by the switching of GSC. This controller presents the following transfer function:

$$G_{PIR}(s) = k_p + \sum_h \frac{2k_i s}{s^2 + 2\omega_f s + (h\omega_s)^2} \qquad (41)$$

Where h is the harmonic order, ω_s is the angular frequency of fundamental signal and ω_f is the desired frequency bandwidth. To obtain the gains of the controller, root locus method was used. The parameters and values of the PIR controller are shown in TABLE I.

Table 1 - Proportional Integral Resonant Parameters

Parameters	Values
k_p	-200
k_i	-4000
Settling time T_s	0.03 s
ω_f	5 rad/s
ω_s	377 rad/s

Source: Authors.

The PIR controller parameters in (41) give:

$$G_{PIR\,1}(s) = \frac{8000}{s^2 + 10s + (1*377)^2} \qquad (42)$$

$$G_{PIR_5}(s) = \frac{8000}{s^2 + 10s + (5*377)^2} \quad (43)$$

$$G_{PIR_7}(s) = \frac{8000}{s^2 + 10s + (7*377)^2} \quad (44)$$

$$G_{PIR_{11}}(s) = \frac{8000}{s^2 + 10s + (11*377)^2} \quad (45)$$

$$G_{PIR_{13}}(s) = \frac{8000}{s^2 + 10s + (13*377)^2} \quad (46)$$

Thus, the current control scheme proposed in this paper using proportional integral resonant is showed in Figure 6.

Figure 6. GSC current control scheme.

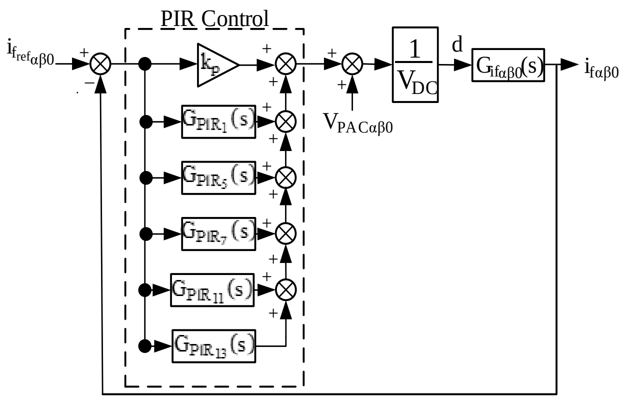

Source: Author

The frequency response of the open-loop transfer function is illustrated in Figure 7.

Figure 7. Bode diagram of GSC current controller.

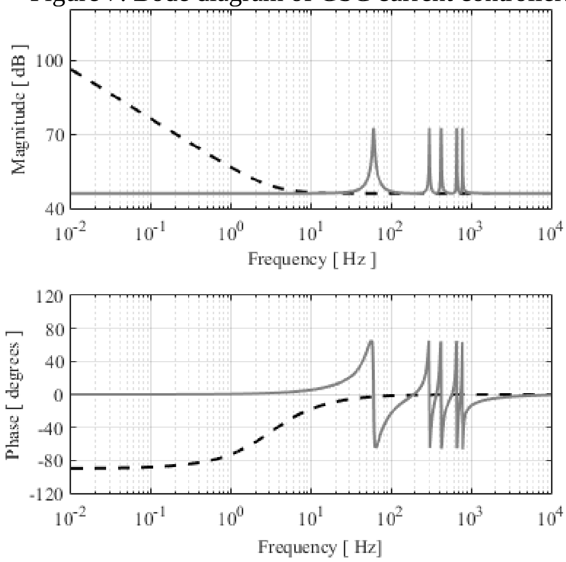

Source: Author

Active Power Filter

The control loop of GSC current in Figure 5 is modified by the insertion of the distorted current generated by the non-linear load at PCC, which supplies new reference currents for harmonic compensation i_{fd}^{*} and i_{fq}^{*}:

$$i_{fd}^{*}= i_{fd}^{ref} - i_{Lhd} \quad (47)$$

$$i_{fq}^{*}= i_{fq}^{ref} - i_{Lhq} \quad (48)$$

Where i_{Lhd} and i_{Lhq} are the harmonic components of load current in d-q axis and i_{fd}^{ref} and i_{fq}^{ref} are the outputs of external control loop.

The harmonic components are identified and isolated by the scheme shown in Figure 8, so that Figure 9 shows the proposed control scheme of active power filtering in the GSC with the harmonic current subtraction.

Figure 8. Harmonic current isolator.

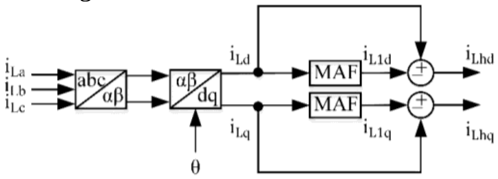

Source: Author

Figure 9. GSC current control scheme with APF.

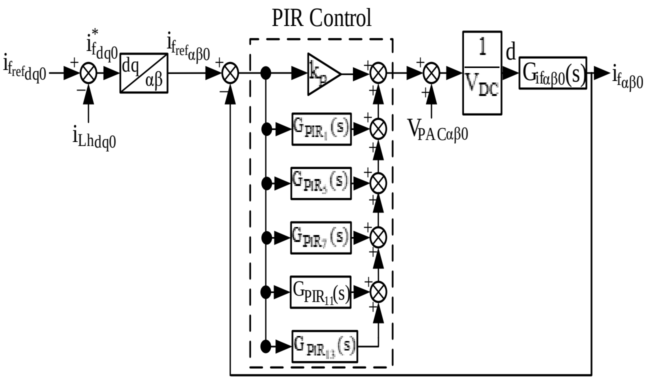

Source: Author

The external control loop of DC voltage in GSC is obtained from:

$$i_{fd} = -\frac{2CV_{DC}}{3V_{PCC_d}}\frac{de_{VDC}}{dt} + \frac{2V_{DC}}{3V_{PCC_d}} i_{cm} \qquad (49)$$

Where e_{VDC} is the PI controller error i_{cm} is the machine side converter DC current, i_0 is the grid side converter DC current and i_c is the capacitor DC link current.

$$i_{cm} = i_0 - i_c \qquad (50)$$

The regulation of system power factor can be achieved by controlling reactive power at PCC, which consists of PCC voltage-oriented vector control technique. Thus, reactive power is obtained from:

$$Q_e = \frac{3}{2}\left(-V_{PCC_d} i_{fq} + V_{PCC_q} i_{fd}\right) \qquad (51)$$

As PCC voltage vector is oriented by direct axis, V_{PCC_q} is null and (51) can be rewritten as:

$$Q_e = -\frac{3}{2} V_{PCC_d} i_{fq} \qquad (52)$$

And isolating quadrature current derivative, one can obtain:

$$\frac{di_{fq}}{dt} = \frac{2}{3V_{PCC_d}} \frac{de_{Q_e}}{dt} \qquad (53)$$

Where e_{Q_e} is the PI controller error.

Computational Results

The system shown in Figure 1 was modeled and simulated in Matlab/Simulink® associated with SimPowerSystem toolbox to analyze the control strategy proposed by DFIG with APF system. The electric grid and GSC parameters used in the simulation are shown in Appendix.

Aiming to evaluate and validate the proposed control system, three cases of operation are studied. In case 1, there are different resistive-inductive loads at the PCC switched along time to investigate reactive compensation. In case 2, the system feeds a 1.1 kW squirrel cage induction motor with torque variation in its axis to analyze the dynamic variation of power factor. In case 3, there is a three-phase diode bridge rectifier with inductive filter as input feeding different loads profile. From case 3, one can observe the active power filtering of grid current to mitigate 5ª, 7ª, 11ª e 13ª harmonics. For all three cases, it was used the same variable wind profile, illustrated in Figure 10.

Figure 10. Available and controlled power from wind.

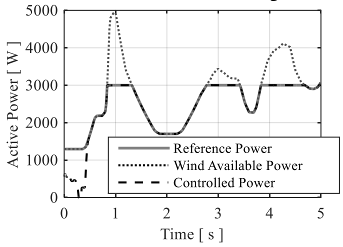

Source: Author

By analyzing Figure 10, it is possible to notice that the maximum power was extracted from the wind, which is the rated power of 3.0 kW fixed by DFIG rotor. To speeds above this limit, the pitch angle control well known in literature has operated to protect the turbine.

Case 1

In this case, different resistive-inductive loads were connected at the PCC as shown in TABLE II.

Table 2 - RL Load Parameters

Case	Load	Time (s)	Active Power (W)	Reactive Power (var)
1	RL	$0.0 \leq t < 1.0$	200	300
		$1.0 \leq t < 2.0$	2000	600
		$2.0 \leq t < 3.0$	3000	0
		$3.0 \leq t < 4.0$	0	700
		$4.0 \leq t < 5.0$	2000	900

Source: Author

The active power balance of the system can be observed in Figure 11. It shows that from 1.6 to 3.0 s, both grid and the DFIG deliver active power to the load. From 3.0 to 4.0 s, the active power demanded from the load is zero, then all the active power generated from DFIG is delivered to the grid. From 4.0 to 5.0 s, once more the DFIG supplies energy to the load and provides its exceeding to the electric grid. Besides, one can notice the dynamic behavior between the generator and the grid as the wind speed profile varies, which guarantees balanced power. Figure 12 shows the behavior of PCC voltage and grid current of phase *a* during the dynamic control, which shows a phase opposition between them when electric grid is absorbing power.

Figure 11. Active power balance of case 1.

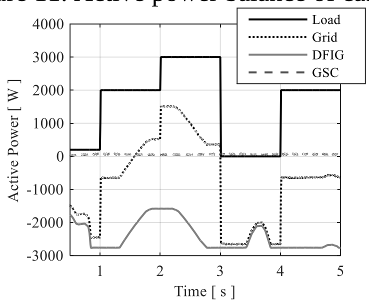

Source: Author

Figure 12. Phase *a* PCC voltage and grid current of case 1.

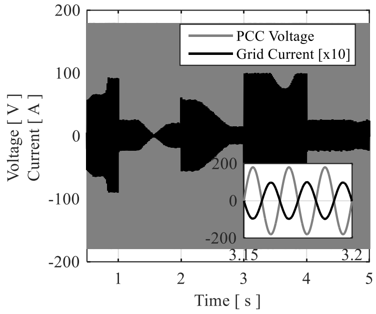

Source: Author

Figure 13 and Figure 14 show the reactive power balance of the system, where it can be observed its compensation, once the reactive energy demanded by the load is fully provided by the GSC. In other words, both reactive energy from electric grid and from DFIG is around zero, with low oscillation of ± 10 var.

Figure 13. Reactive power balance of case 1.

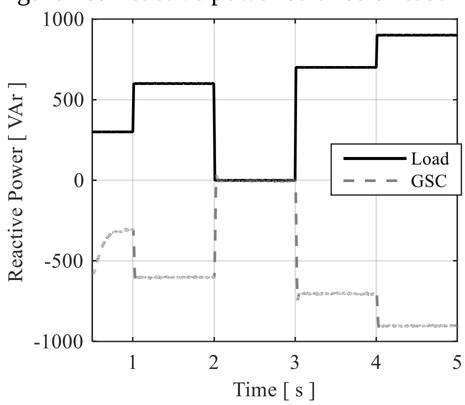

Source: Author

The energy peaks of Figure 14 are derived from load switching. DC link voltage can be observed in Figure 15. The system keeps its value in 400 volts and presents low oscillation around the operation point, considering the different load switches. The usage of PIR controllers guarantees the low variation of ± 0.5 V.

Figure 14. Reactive power from grid and DFIG of case 1.

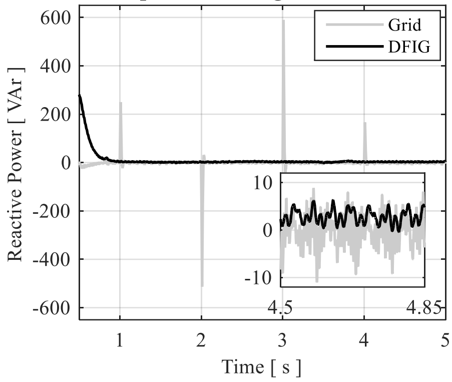

Source: Author

Figure 15. DC link voltage of case 1.

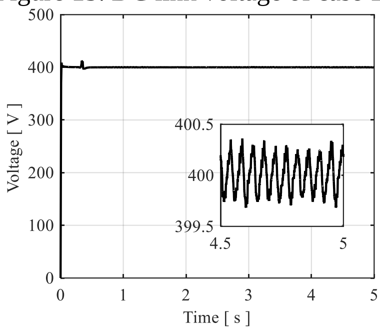

Source: Author

Case 2

In this case, there is torque variation on the 1.1 kW squirrel cage induction motor axis, as shows Figure 16, which allows to analyze power factor dynamically by varying active power consumption.

Figure 16. Torque applied to the induction motor axis of case 2.

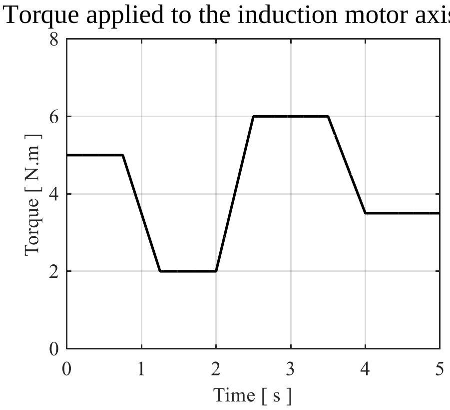

Source: Author

The active power balance of the system is shown in Figure 17, where one can observe that DFIG is able to supply active power demanded by induction motor and yet provides the exceeding energy to electric grid. Figure 18 shows the behavior of PCC voltage and grid current of phase *a* during the dynamic control of reactive compensation, which shows a phase opposition between them when the grid is absorbing power.

The reactive power demanded by induction machine is shown in Figure 19. Once back-to-back converter is designed to compensate up to 30% of DFIG rated power, GSC was able to delivery only 900 from 1300 var demanded by load. It is noteworthy that the control loop of reactive energy was designed to compensate partially or completely the reactive energy of the system.

Figure 17. Active power balance of case 2.

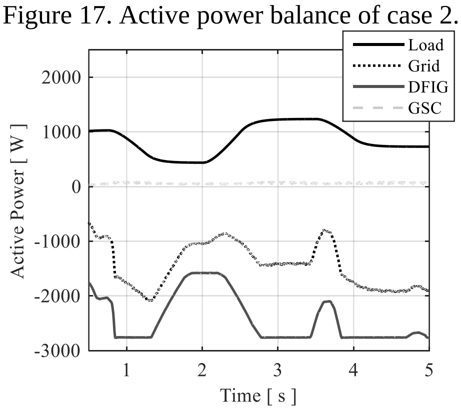

Source: Author

Figure 18. Phase *a* PCC voltage and grid current of case 2.

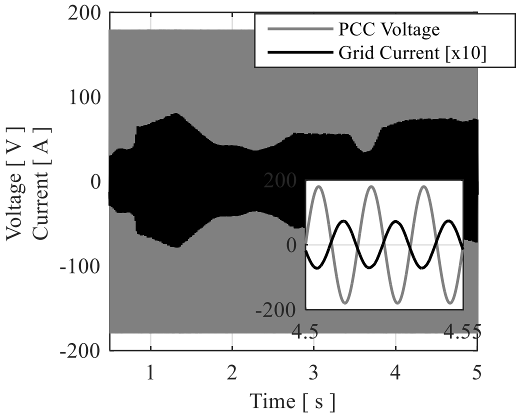

Source: Author

Figure 19. Reactive power balance of case 2.

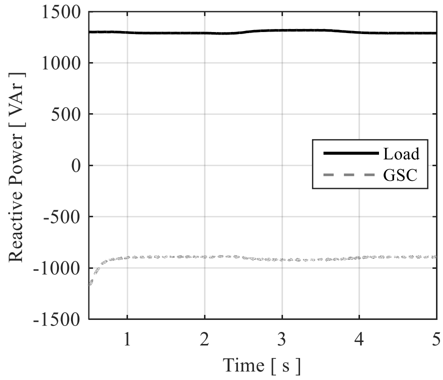

Source: Author

Figure 20. Reactive power from grid and DFIG of case 2.

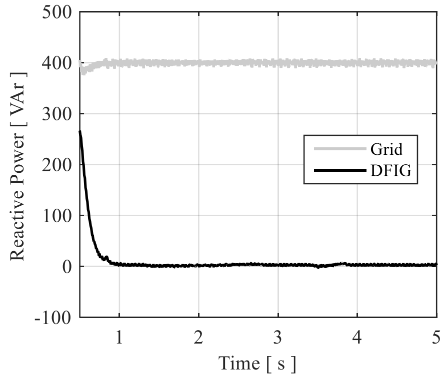

Source: Author

DC link voltage can be observed in Figure 21. The system regulates it in 400 volts, with oscillation up to 0.5 volts. One of the advantages of PIR is the assistance to keep low oscillation of dc link voltage around 400 V.

Figure 21. DC link voltage of case 2.

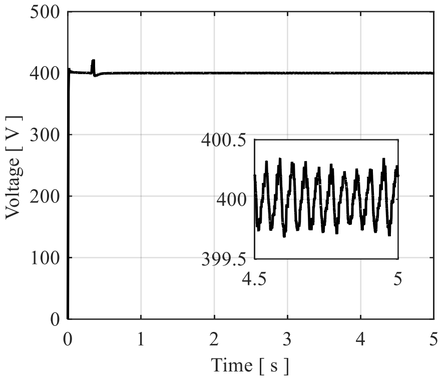

Source: Author

Case 3

Finally, in case 3, the system supplies energy to a three-phase diode bridge rectifier so that GSC control performs active power filtering of electric grid current. In order to discuss and analyze the effectiveness of the proposed method in harmonic mitigation, it was simulated different loads at dc side of rectifier with and without APF, as shown in TABLE III.

Table 3 - Rectifier Load Parameters

Case	Time (s)	R (Ω)	L (mH)	C (μF)
	0.0 ≤ t < 2.0	80	0	0
3	2.0 ≤ t < 3.5	80	50	0
	3.5 ≤ t < 5.0	80	0	1000

Source: Author

Case 3.1 – Without APF

The active power balance of the system can be observed in Figure 22. Active power balance of case 3.1 - without APF., where one can notice that the oscillation derived from the non-linearity of the load connected at PCC was reflected in the power of the grid. Figure 23 shows the behavior of PCC voltage and grid current of phase *a* during the dynamic control of reactive compensation, which shows a phase opposition between them when the grid is absorbing power, even with the non-sinusoidal profile of the grid current.

Figure 22. Active power balance of case 3.1 - without APF.

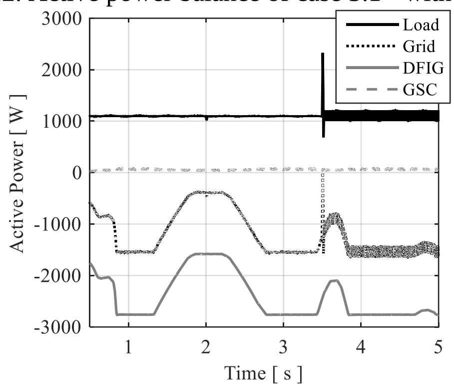

Source: Author

The reactive power balance of the system is shown in Figure 24 and Figure 25. By analyzing Figure 24, one can notice that GSC compensates the reactive energy demanded by the load, however, in the same way with active power, the oscillation due to the non-linear profile of the load is reflected to the grid, creating a variation of almost 50 VAr.

Figure 23. Phase *a* PCC voltage and grid current of case 3.1 – without APF.

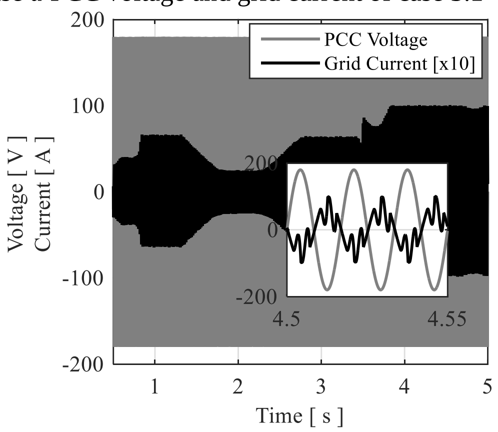

Source: Author

Figure 24. Reactive power balance of case 3.1 – without APF.

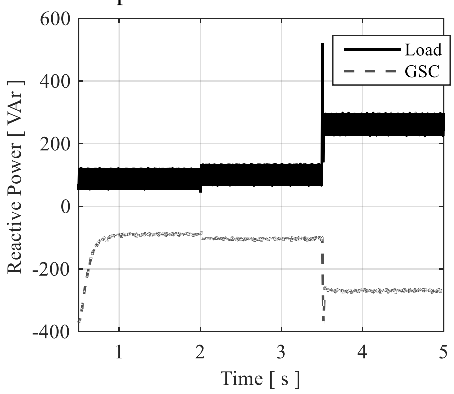

Source: Author

Figure 25. Reactive power from grid and DFIG of case 3.1 – without APF.

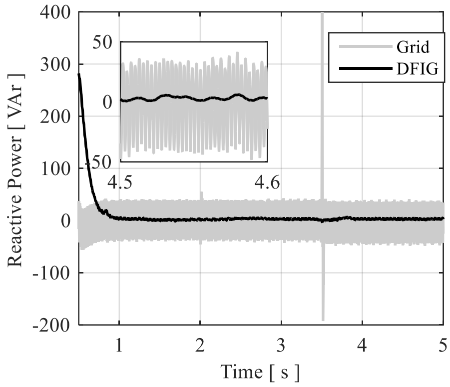

Source: Author

The waveforms of electric current of load, DFIG, grid and GSC for different load profiles in the three-phase rectifier dc side are shown in Figure 26, Figure 28 and Figure 30. Without the active power filtering, the grid current presented a non-sinusoidal highly distorted behavior. This distortion in the current may cause as well voltage distortion to other consumers connected at PCC, making the power quality poor in this point.

The harmonic spectrum of grid current considering the different load profiles is shown in Figure 27, Figure 29 and Figure 31 It can be observed that the grid current presents a high harmonic content. This harmonic content may cause problems of power quality, as previously mentioned, such as increase of distorted power and power factor deterioration.

Figure 26. PCC currents from 1.2 to 1.23 s of case 3.1 - without APF.

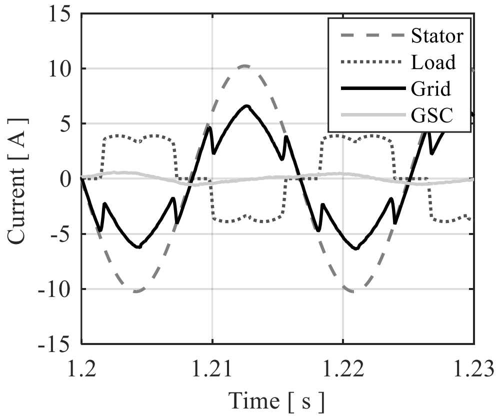

Source: Author

Figure 27. Grid current THD from 1.2 to 1.23 s of case 3.1 - without APF.

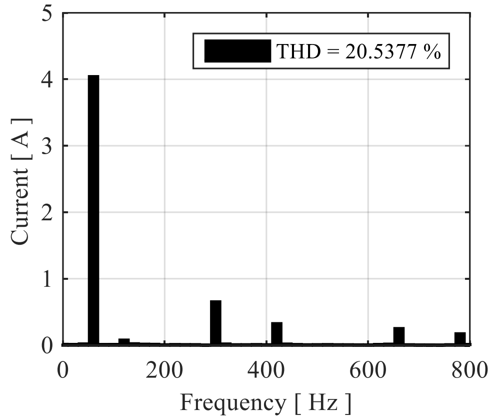

Source: Author

Figure 28. PCC currents from 2.2 to 2.23 s of case 3.1 - without APF.

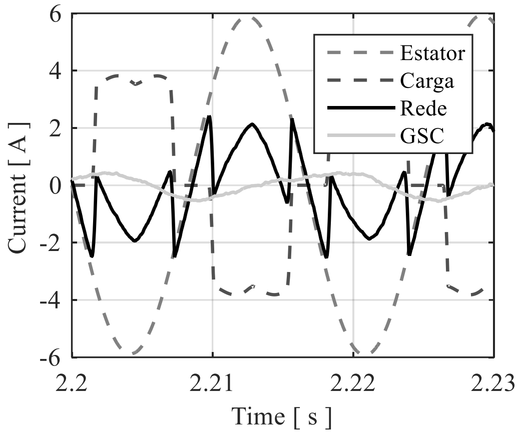

Source: Author

Figure 29. Grid current THD from 2.2 to 2.23 s of case 3.1 - without APF.

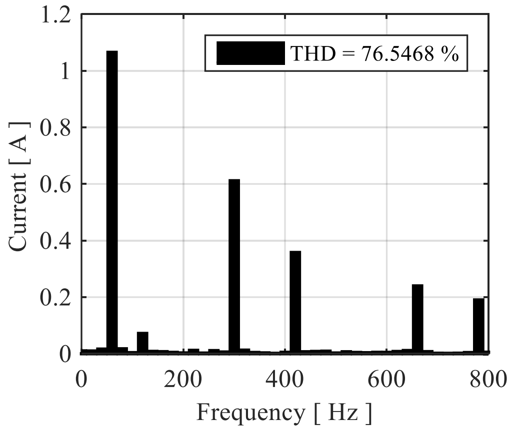

Source: Author

Figure 30. PCC currents from 4.2 to 4.23 s of case 3.1 - without APF.

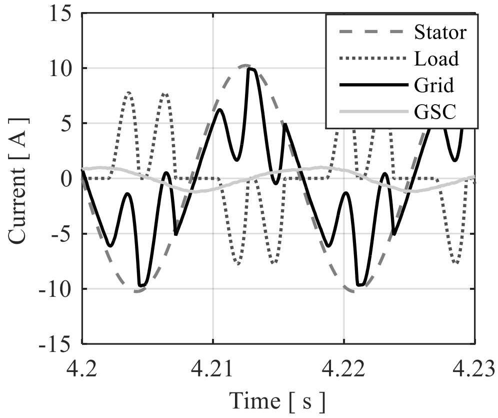

Source: Author

Figure 31. Grid current THD from 4.2 to 4.23 s of case 3.1 - without APF.

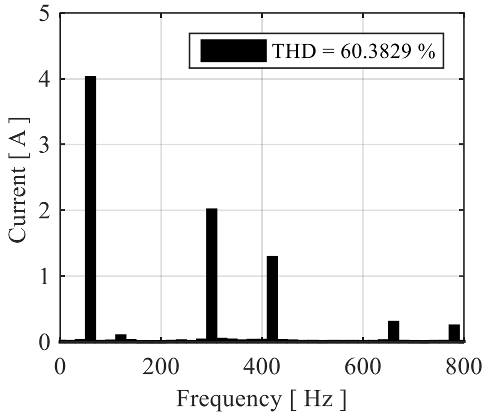

Source: Author

Case 3.2 – With APF

The active power balance of the system can be observed in Figure 32, where it can be observed that the oscillation derived from the non-linearity of the load connected at PCC was reflected now in GSC, differently from what happens to the same system without APF. This causes a decrease in the oscillation of the active power absorbed by the grid, improving the power quality. Besides, it shows the dynamic behavior between active power from grid and the generator. Figure 33 shows the behavior of PCC voltage and grid current of phase *a* during the dynamic control of reactive compensation, which shows a phase opposition between them when the grid is absorbing power, as well as the grid current presents less distortion when compared to the same system without APF.

Figure 32. Active power balance of case 3.2 – with APF.

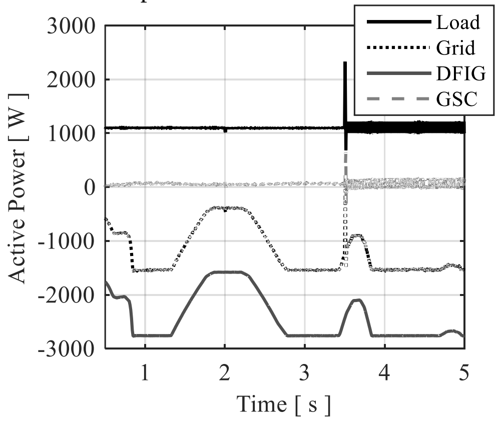

Source: Author

Figure 33. Phase *a* PCC voltage and grid current of case 3.2 – with APF.

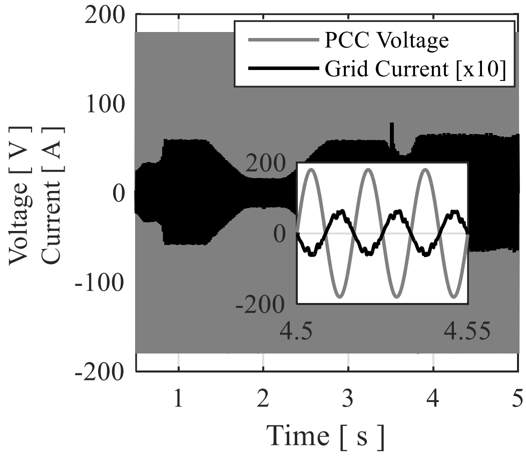

Source: Author

The behavior of the system can also be observed through the dc link voltage, shown in Figure 34. The voltage value was kept stable around 400 V during the load switches, with fast transient response around 0.1 s and low oscillation in the region of ± 2 V. Thus, the proposed method of control with APF of the grid current is satisfactory and the stability of the dc link was possible due to the replace of PI controllers by the PIR ones.

Figure 34. DC link voltage of case 3.2 – with APF.

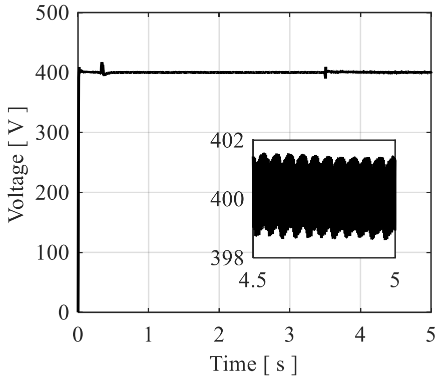

Source: Author

The reactive power balance of the system is shown in Figure 35 and Figure 36. By analyzing Figure 35, one can notice that GSC compensates the reactive energy demanded by the load and, consequently, the reactive power supplied by the grid and by the DFIG stator is almost null, which decreases the oscillation of reactive power from the grid into until five times when compared to the same case without APF. Besides, all the oscillation from the non-linearity of the load is reflected to GSC. In this way, power factor is kept close to unity.

Figure 35. Reactive power balance of case 3.2 – with APF.

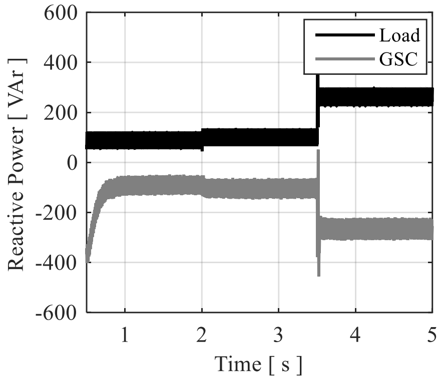

Source: Author

Figure 36. Reactive power from grid and DFIG of case 3.2 – with APF.

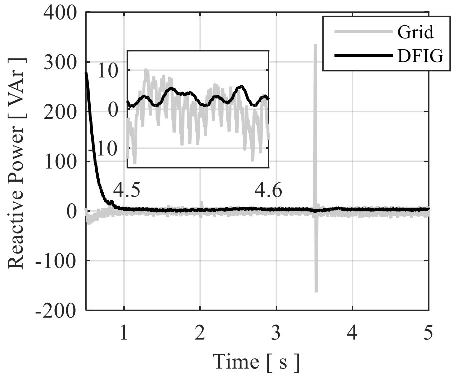

Source: Author

Beyond that, from Figure 36 it can be noticed the low magnitude variation of reactive power of the grid and the generator, about 10 VAr, which shows the efficiency of the proposed control method.

The waveforms of electric current of load, DFIG, grid and GSC for different load profiles in the three-phase rectifier dc side are shown in Figure 37, Figure 39 and Figure 41. Due to the active power filtering and the harmonic compensation, the waveform of grid current is close to sinusoidal and GSC absorbs the harmonic content from the load. Besides, Figure 39 shows that grid current is the smallest one and more susceptible to noises, which explains its waveform less sinusoidal.

The harmonic spectrum of grid current considering the different load profiles is shown in Figure 38, Figure 40 and Figure 42.

Figure 37. PCC currents from 1.2 to 1.23 s of case 3.2 – with APF.

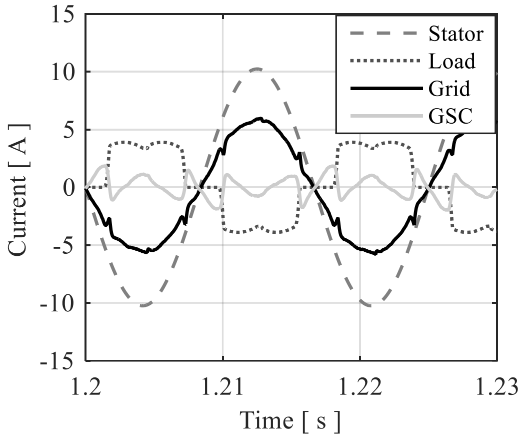

Source: Author

Figure 38. Grid current THD from 1.2 to 1.23 s of case 3.2 – with APF.

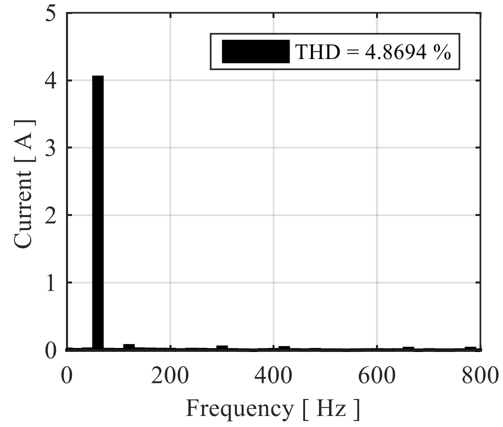

Source: Author

Figure 39. PCC currents from 2.2 to 2.23 s of case 3.2 – with APF.

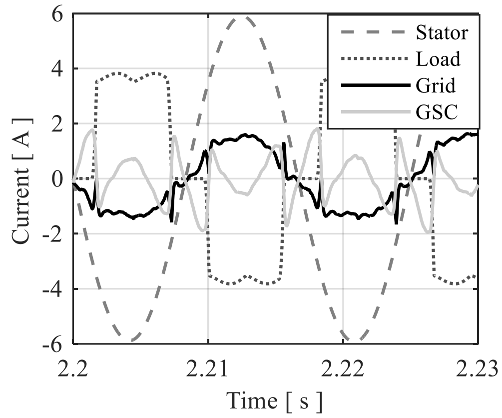

Source: Author

Figure 40. Grid current THD from 2.2 to 2.23 s of case 3.2 – with APF.

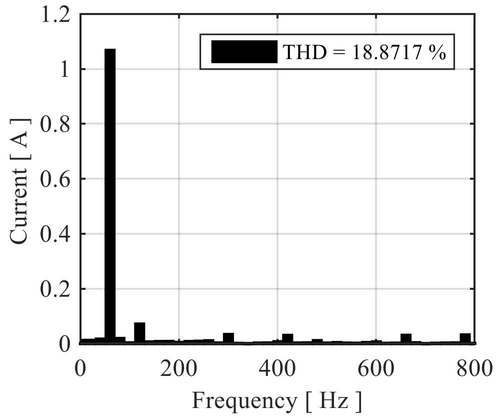

Source: Author

Figure 41. PCC currents from 4.2 to 4.23 s of case 3.2 – with APF.

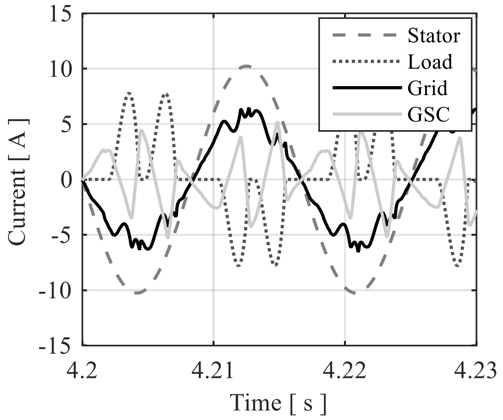

Source: Author

Figure 42. Grid current THD from 4.2 to 4.23 s of case 3.2 – with APF.

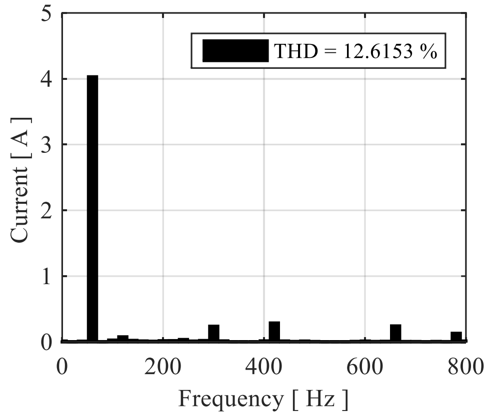

Source: Author

Comparing the case without APF to the case with APF, there was a significant decrease in the grid current THD, making its profile almost sinusoidal and improving power quality.

Comparing all the harmonic spectra of cases 3.1 and 3.2, one can notice the efficiency of APF implementation once the harmonic content of grid current presents reduction in all three cases of different loads in dc side of rectifier, as follows in TABLE IV:

Table 4 - Comparison of grid current thd with and without apf.

Time (s)	THD without APF (%)	THD with APF (%)
$1.20 \leq t < 1.23$	20.5377	4.8694
$2.20 \leq t < 2.23$	76.5468	18.8717
$4.20 \leq t < 4.23$	60.3829	12.6153

Source: Author

From the concepts of Currents' Physical Components theory presented in Section III, it is possible to analyze and interpret the system WT-DFIG operation when it is submitted to a non-linear load, as in case 3. TABLE V shows the power components and power factor of the system without and with APF in different times considering the different loads.

Table 5 - CPC theory power components

Time (s)		Without APF	With APF
t = 1.0	P_a (W)	1545.170	1538.504
	Q_r (VAr)	294.108	91.756
	D_s (VA)	300.126	134.332
	D_G (VA)	4.222	3.597
	D_u (VA)	511.87	173.137
	S (VA)	1680.939	1556.731
	PF (P_a÷S)	0.919	0.988
t = 3.0	P_a (W)	1552.201	1546.215
	Q_r (VAr)	300.668	92.978
	D_s (VA)	320.067	138.998
	D_G (VA)	4.686	3.840
	D_u (VA)	503.899	171.593
	S (VA)	1690	1564.674
	PF (P_a÷S)	0.918	0.988
t = 4.25	P_a (W)	1565.701	1531.607
	Q_r (VAr)	1083.535	283.067
	D_s (VA)	251.206	168.348
	D_G (VA)	3.296	4.275
	D_u (VA)	1302.606	335.496
	S (VA)	2320.639	1602.144
	PF (P_a÷S)	0.675	0.956

Source: Author

From TABLE V, once more the proposed method of active power filtering stands out with a significant improvement of power factor, with an increase of 0.675 to 0.956 in t = 4.24 s, which was the worst case.

CONCLUSION

This study addressed the research question of whether an appropriate control strategy applied to a wind generation system based on a doubly fed induction generator (DFIG), connected to the distribution grid, could effectively improve power quality at the point of common coupling under different load conditions, including nonlinear loads. To answer this question, a wind energy conversion system equipped with a back-to-back converter was modeled and simulated in the Matlab/Simulink® environment using the SimPowerSystem toolbox, allowing the analysis of system dynamics under varying load profiles.

The simulation results demonstrated that the proposed grid-side converter (GSC) control strategy successfully regulated the DC-link voltage, exhibiting good transient performance and low oscillation magnitude. Moreover, the independent control of active and reactive power was achieved. The use of proportional–integral–resonant (PIR) controllers in the current control loop proved effective in mitigating harmonic components arising from switching effects and nonlinear loads, maintaining DC-link voltage stability. In addition, the proposed active power filtering (APF) technique significantly improved the grid current waveform, resulting in a nearly sinusoidal profile and a power factor close to unity. These results confirm that the proposed control strategy satisfactorily meets the objectives of the research and effectively enhances the power quality of the studied wind generation system.

From a broader perspective, the findings contribute to both society and academia. In practical terms, the proposed approach supports the integration of wind energy systems into distribution networks by reducing harmonic distortion and improving power factor, thereby increasing grid reliability and efficiency. From an academic standpoint, this work provides a comprehensive modeling framework and a validated control strategy for DFIG-based wind systems, contributing to ongoing research on power quality improvement and advanced converter control techniques in renewable energy applications.

Despite the positive outcomes, this research is subject to some limitations. The analysis was restricted to simulation-based results, without experimental validation, and the adopted back-to-back converter topology does not allow the mitigation of homopolar harmonic components, such as the 3rd and 9th harmonics. Therefore, future work should focus on experimental implementation and validation of the proposed control strategy, as well as on the incorporation of an additional converter leg to enable the mitigation of homopolar harmonics and further improve power quality performance.

REFERENCES

ABAD, G. (Ed.). **Doubly fed induction machine: modeling and control for wind energy generation**. Hoboken: IEEE Press, 2011. Acesso em: 03 mar. 2025.

ACKERMANN, T. (Ed.). **Wind power in power systems**. 2. ed. Chichester; Hoboken: Wiley, 2012. Acesso em: 10 fev. 2025.

AKAGI, H.; SATO, H. **Control and performance of a doubly-fed induction machine intended for a flywheel energy storage system**. **IEEE Transactions on Power Electronics**, Piscataway, v. 17, n. 1, p. 109–116, jan. 2002. Acesso em: 11 mar. 2024.

BOSE, B. K. **Modern power electronics and AC drives**. Upper Saddle River: Prentice Hall,

2001. Acesso em: 17 abr. 2024.

BOUTOUBAT, M.; MOKRANI, L.; MACHMOUM, M.; AUGER, F. **Selective harmonics compensation using a WECS equipped by a DFIGURE** In: **IECON 2012 – 38th Annual Conference on IEEE Industrial Electronics Society**, 2012. Anais […]. Piscataway: IEEE, 2012. p. 745–750. Acesso em: 08 fev. 2025.

BUBSHAIT, A. S.; MORTEZAEI, A.; SIMÕES, M. G.; BUSARELLO, T. D. C. **Power quality enhancement for a grid connected wind turbine energy system**. **IEEE Transactions on Industry Applications**, Piscataway, v. 53, n. 3, p. 2495–2505, maio 2017. Acesso em: 15 mar. 2025.

CLARKE, E. **Circuit analysis of A-C power systems: symmetrical and related components**. New York: Wiley, 1943. v. 1. Acesso em: 21 jan. 2025.

KRAUSE, P.; WASYNCZUK, O.; SUDHOFF, S. D.; PEKAREK, S. **Analysis of electric machinery and drive systems**. Hoboken: John Wiley & Sons, 2013. Acesso em: 25 maio 2025.

LÓPEZ-NÚÑEZ, A. R.; MINA, J. D.; AGUAYO, J.; CALDERÓN, G. **Proportional integral resonant controller for current harmonics mitigation in a wind energy conversion system**. In: **International Conference on Power Electronics (CIEP)**, 13., 2016. Anais […]. Piscataway: IEEE, 2016. p. 232–237. Acesso em: 07 abr. 2025.

MEEGAHAPOLA, L.; FLYNN, D. **Impact on transient and frequency stability for a power system at very high wind penetration**. In: **IEEE PES General Meeting**, 2010. Anais […]. Piscataway: IEEE, 2010. p. 1–8. Acesso em: 30 mar. 2024.

MOREIRA, A. B.; BARROS, T. A. S.; TEIXEIRA, V. S. C.; RUPPERT, E. **Power control for wind power generation and current harmonic filtering with doubly fed induction generator**. **Renewable Energy**, Oxford, v. 107, p. 181–193, jul. 2017. Acesso em: 22 jan. 2025.

NAIDU, N. K. S.; SINGH, B. **Doubly fed induction generator for wind energy conversion systems with integrated active filter capabilities**. **IEEE Transactions on Industrial Informatics**, Piscataway, v. 11, n. 4, p. 923–933, ago. 2015. Acesso em: 09 jun. 2025.

NAM, T. Q.; HOONG, C. F.; YI, T.; PENG, W. **A control strategy to compensate for current and voltage measurement errors in three-phase PWM rectifiers**. In: **IEEE Energy Conversion Congress and Exposition (ECCE)**, 2017. Anais […]. Piscataway: IEEE, 2017. p. 4601–4608. Acesso em: 13 maio 2025.

PENA, R.; CLARE, J. C.; ASHER, G. M. **Doubly fed induction generator using back-to-back PWM converters and its application to variable-speed wind-energy generation**. **IEE Proceedings – Electric Power Applications**, Londres, v. 143, n. 3, p. 231–241, maio 1996. Acesso em: 28 fev. 2025.

RASHID, M. H. **Power electronics: circuits, devices & applications**. 4. ed. Upper Saddle River: Pearson, 2013. Acesso em: 05 maio 2025.

SEYOUM, D.; GRANTHAM, C.; RAHMAN, M. F. **Simplified flux estimation for control application in induction machines**. In: **IEEE International Electric Machines and Drives Conference (IEMDC)**, 2003. Anais […]. Piscataway: IEEE, 2003. v. 2, p. 691–695. Acesso em: 06 abr. 2024.

SINGH, B.; NAIDU, N. K. S. **Direct power control of single VSC-based DFIG without rotor position sensor**. **IEEE Transactions on Industry Applications**, Piscataway, v. 50, n. 6, p. 4152–4163, nov. 2014. Acesso em: 02 abr. 2024.

SUN, D.; WANG, X. **Low-complexity model predictive direct power control for DFIG under both balanced and unbalanced grid conditions**. **IEEE Transactions on Industrial Electronics**, Piscataway, v. 63, n. 8, p. 5186–5196, ago. 2016. Acesso em: 27 fev. 2025.

SUN, D.; WANG, X.; NIAN, H.; ZHU, Z. Q. **A sliding-mode direct power control strategy for DFIG under both balanced and unbalanced grid conditions using extended active power**. **IEEE Transactions on Power Electronics**, Piscataway, v. 33, n. 2, p. 1313–1322, fev. 2018. Acesso em: 19 maio 2025.

TAPIA, A.; TAPIA, G.; OSTOLAZA, J. X.; SAENZ, J. R. **Modeling and control of a wind turbine driven doubly fed induction generator**. **IEEE Transactions on Energy Conversion**, Piscataway, v. 18, n. 2, p. 194–204, jun. 2003. Acesso em: 12 abr. 2024.

TIAN, X.; TANG, H.; LI, Y.; CHI, Y.; SU, Y. **Dynamic stability of weak grid connection of large-scale DFIG based on wind turbines**. **Journal of Engineering**, Londres, v. 2017, n. 13, p. 1092–1097, 2017. Acesso em: 18 abr. 2024.

TODESCHINI, G.; EMANUEL, A. E. **Wind energy conversion systems as active filters: design and comparison of three control methods**. **IET Renewable Power Generation**, Londres, v. 4, n. 4, p. 341–353, jul. 2010. Acesso em: 14 fev. 2024.

WANG, X.; SUN, D.; ZHU, Z. Q. **Resonant-based backstepping direct power control strategy for DFIG under both balanced and unbalanced grid conditions**. **IEEE Transactions on Industry Applications**, Piscataway, v. 53, n. 5, p. 4821–4830, set. 2017. Acesso em: 20 mar. 2025.

APPENDIX

The DFIG system, electric grid and the GSC parameters that are used for simulation tests are summarized in TABLE VI, TABLE VII and TABLE VIII respectively.

Table 6 - DFIG parameters

Parameter	Value
Rated Power	3.0 kW
Nominal Voltage	220 V
Frequency	60 Hz
Rotor Resistance R_r'	0.816 Ω
Stator Resistance R_s	0.435 Ω
Rotor Inductance L_r'	2.0 mH
Stator Inductance L_s	4.0 mH
Mutual Inductance L_m	69.31 mH
Moment of Inertia J	0.089 kg.m²

Source: Author

Table 7 - Electric grid parameters

Parameter	Value
Line Voltage	220 V
Coupling Inductor L_g	0.01 mH
Frequency	60 Hz

Source: Author

Table 8 - GSC Parameters

Parameter	Value
Filter Inductor L_f	10.0 mH
Filter Resistance R_f	0.1 Ω
DC link Capacitor C	1.0 mF

Source: Author